2004

Hydrogen Peroxide Detection at Electrochemically and Sol-Gel Derived Ir Oxide Films

Birss, Viola I.; Elzanowska, Hanna; Abu-Irhayem, Erfan; Skrzynecka, Beata

Wiley-VHC

Elzanowska, H., Abu-Irhayem, E., Skrzynecka, B. and Birss, V. I. (2004). "Hydrogen Peroxide Detection at Electrochemically and Sol-Gel Derived Ir Oxide Films". Electroanalysis, Vol. 16, NO. 6: 478-490.

http://hdl.handle.net/1880/44936

journal article

Full Paper

Hydrogen Peroxide Detection at Electrochemically and Sol-Gel Derived Ir Oxide Films

Hanna Elzanowska,[a] *Erfan Abu-Irhayem*,[b] *Beata Skrzynecka*,[a] *Viola I. Birss**[b]*

[a] Department of Chemistry, University of Warsaw, 02–093 Warsaw, Poland
[b] Department of Chemistry, University of Calgary, Calgary, Alberta, Canada T2N 1N4
*e-mail: birss@ucalgary.ca

Received: November 14, 2002
Final version: March 28, 2003

Abstract

Ir oxide (IrOx) films, formed electrochemically on bulk Ir metal (Ir/IrOx) and also on sol-gel (SG) derived non-silica based nanoparticulate Ir, have been studied as material useful for the detection of hydrogen peroxide, with possible application as a glucose biosensor. H_2O_2 reduction and oxidation on Ir/IrOx and SG-derived IrOx films, deposited on various substrates such as Pt, Ir and GC, have been compared to the H_2O_2 behavior at the bare substrate. It was found that H_2O_2 reduction proceeds on the underlying electrode substrate, while H_2O_2 oxidation is independent of the nature of the substrate, therefore occurring via the IrOx film. The reactivity of IrOx towards H_2O_2 oxidation is similar to that seen at Pt, although IrOx has the additional advantages of excellent stability, insensitivity to common interfering substances, biocompatibility and a linear range of detection, up to at least 12 mM H_2O_2. At micromolar concentrations of H_2O_2, a second mode of detection, involving the catalyzed growth of IrOx films at Ir substrates, can be employed. These two methods of H_2O_2 analysis (oxidation/reduction and enhanced IrOx growth) can also be employed for glucose detection using IrOx-based glucose biosensors.

Keywords: Hydrogen peroxide, Glucose biosensor, Sol-gel, Sol, Nanoparticulate, Cyclic voltammetry, Ir oxide, Ir metal, Glucose

1. Introduction

There are many industrial applications of H_2O_2 sensors [1], including wine and food production, pulp and paper bleaching, sterilization, the oxidation of organic substances, etc. The renewed interest in H_2O_2 detection, observed over the last decade, is related not only to the increased awareness of environmental hazards and the need for safer procedures, but also to new applications of H_2O_2, e.g., in precious metal extraction from the associated ores [1]. In the area of biosensors, there is a continuing interest [2] in H_2O_2 detection in 'first generation' biosensors containing oxidases, particularly glucose biosensors involving glucose oxidase (GOx), in which H_2O_2 is produced in an enzymatic reaction involving glucose, GOx, and molecular oxygen. Despite significant progress made in developing mediator-based 'second generation' biosensors, which employ a mediator that competes with oxygen in the enzymatic reaction, problems related to the immobilization of the mediator, its toxicity, stability, and mediator leakage over extended period of time from the electrode remain unsolved [2]. H_2O_2 detection is used in implantable glucose biosensors [2] and in newly developed transdermal devices, which require H_2O_2 detection in micromolar concentrations [2, 3]. Another important application of H_2O_2 sensors is in monitoring it at micromolar concentrations in human polymorphonuclear leukocytes [4]. These developments contribute to the continuing interest in 'first generation' biosensors and the detection of H_2O_2 on various types of electrodes.

The electrode traditionally used [5–12] for the detection of H_2O_2 is Pt, known for its excellent electrocatalytic properties towards H_2O_2 oxidation. Pt electrodes, however, are prone to poisoning and require meticulous cleaning pretreatment procedures [10–12]. Further, a resistive oxide film will grow on Pt with time at constant potential, altering the electrode response, and thus care must be taken to allow the oxide film to reach steady-state conditions before measuring the H_2O_2 oxidation current. Also, despite the relatively low H_2O_2 detection potential (usually 0.6 V vs. SCE), problems arise with concurrent oxidation of common interfering species, such as ascorbic acid, urea, paracetamol, etc. [2].

Therefore, a variety of other types of electrodes have been used for H_2O_2 detection, including metallic or alloy electrodes such as Pt/Ir [10], Pd [13], Pd/Au [14, 15], Pd/Ir [16, 17] and also electrodes modified with peroxidase [18], Prussian Blue, an 'artificial peroxidase' [19], and metallized polymer electrodes [20]. Metals and alloys have also been used for the detection of H_2O_2 in a glucose biosensor, formed by the co-deposition of GOx and metals such as Pt [21, 22], Rh [23, 24], Ru [25], Pd [26], Ir [27, 28], and Ru/Pt [29] on carbon paste and carbon fibre electrodes. Similarly, Ir powder has been added to silica sol-gel derived electrodes to form iridium-containing ceramic sensing electrodes [30].

There are also a few examples of the use of metal oxide electrodes in biosensors, including Mn [31], Sn [32] and Ir

  DOI: 10.1002/elan.200402837

oxide [33, 34], while H_2O_2 redox processes have also been studied on W [35, 36] and Ir oxide [37] electrodes. Ir oxide electrodes [33, 34, 37] offer an excellent matrix for both the immobilization of GOx and H_2O_2 detection. The detection potential can be lowered to ca. 0.4 V for H_2O_2 oxidation and to −0.1 V (vs. SCE) for H_2O_2 reduction [33, 34]. Additionally, Ir oxide (IrOx) films [34] and also other oxide electrodes such as Mn oxide [31] are not prone to interferences.

Other positive features of IrOx electrodes include their stability, the rapid, reversible redox reactions of the Ir(+III/IV/V/VI) sites [38–47], the exceptional resistance to dissolution and corrosive changes of the surface structure during in vitro or in vivo potential stimulation [48–49], and their ability to accommodate much more charge than other metals such as Pt [49]. As well, IrOx electrodes have been reported to be biocompatible, based on research carried out by W. F Agnew et al. [50], in which they evaluated the effect of prolonged intracortical electrical stimulation in cats' brains, using activated Ir microelectrode electrical stimulation. The results showed a low incidence of inflammatory reactions in the stimulated sites in the brain, which indicate good biocompatiblity of the electrode material [50]. A further advantage of IrOx films, especially when obtained by oxidation of an Ir surface, relates to the ease of electrodeposition of Ir [51], the facile formation of Ir nanoparticles via sol-gel methods [52, 53] and also the possibility of screen printing of Ir [54]. Relative to Pt, another advantage of the hydrous IrOx electrode is that it reaches its steady-state redox condition extremely rapidly at constant potentials, due to its very rapid (pseudocapacitive) kinetics [42, 43]. IrOx has previously been employed as a neural stimulating electrode [48, 50], as a pH electrode [55–57], and as urea [58, 59], ascorbic acid [60], nitric oxide [61] and glucose biosensors [33, 34].

Recently, we have reported [34] on the immobilization of GOx into IrOx films formed anodically on bulk Ir electrodes. The glucose detection in this biosensor was realized via the oxidative detection of H_2O_2, but the role of IrOx in H_2O_2 oxidation was not examined closely. Taking into consideration that the formation of Pt and Pd oxide has been linked to the catalytic properties of metallic Pt and Pd electrodes towards H_2O_2 oxidation [5–8, 10, 12, 14, 15], the involvement of IrOx in the H_2O_2 redox processes seems likely. However, it has also been suggested [21–29] that the metal plays the key role in the reductive response of a glucose biosensor consisting of Pt, Pd, Ir or Ru co-deposited with GOx.

The present work involves a study of H_2O_2 oxidation and reduction reactions on bare Ir, oxidized Ir (Ir/IrOx) wires and foils, and sol-gel (SG) derived nanoparticulate IrOx films deposited on several substrates (S), e.g., Pt, GC and Ir (S/IrOx). The observed effect of the substrate material, based on well-documented [62] significant differences in the activities of Pt and GC surfaces towards H_2O_2 oxidation and reduction, was used previously [63] to prove that glucose oxidation was being mediated by Ru poly(pyridine) complexes immobilized in a β-cyclodextrin polymer. In the present work, the comparison of the H_2O_2 redox reactions on metallic Ir and on IrOx films formed on bulk Ir, and other substrates has led us to the conclusion that the reduction of H_2O_2 proceeds on oxide-free Pt, Ir, or GC sites, but that the oxidation of H_2O_2 occurs at IrOx. Another example of the active role of IrOx in H_2O_2 reactions is shown in this work by the catalyzed growth of IrOx films in the presence of micromolar concentrations of H_2O_2. The oxidation and reduction of H_2O_2, as well as this observed enhancement in oxide growth, can both be used for the detection of H_2O_2 using Ir/IrOx electrodes. The differences and similarities between the behavior of IrOx and Pt electrodes in H_2O_2 solutions will also be demonstrated, and the application of IrOx electrodes for the electrochemical detection of glucose will also be discussed.

2. Experimental

2.1. Electrodes and Cells

The electrochemical experiments were carried out in a conventional two-compartment glass cell, with one compartment containing the working electrode (WE) and a high surface area Pt mesh counter electrode (CE), and the reference electrode (RE) located in the second compartment, connected through a Luggin capillary. The RE was a saturated calomel electrode (SCE) and all potentials in this paper are referred to the SCE.

Three types of Ir WEs were used: a) 0.05 mm dia. Ir wire (0.16 cm^{-2} geometric area), 99.8% Alfa Aesar, sealed in soft glass tubing; b) glass slides (0.35 cm^2), sputter-coated with an undercoat of Ti to a thickness of ca. 10 nm and then coated with Ir to ca. 80–90 nm using a DV-502A sputtering system; c) Ir sol coated on Ir, Pt, or Au sputtered electrodes (0.35 cm^2), or deposited on GC electrodes (1.5 cm^2). The Ir wire electrodes were flame-cleaned, followed by ultrasonication in 3% H_2O_2 and then electrochemically cleaned by potential cycling in 1 M H_2SO_4 between −0.25 V and 1.3 V (vs. SCE) for 30 min. Sputtered Ir, Pt, and Au electrodes were cleaned, prior to IrOx deposition, by rinsing with methanol and then water.

The solution employed for Ir sol deposition was prepared as described elsewhere [52, 53], using a molar ratio of $IrCl_3$ (or $IrCl_3 \cdot 3H_2O$) to Na ethoxide of 3:1, both dissolved in ethanol. The solution was typically refluxed under Ar for ca. 2 h, stirred under Ar for ca. 20 h, and then filtered. The glass slides, sputter-coated with Pt, Au, or Ir (0.35 cm^2), were then coated with the Ir sol by withdrawal from the solution at a constant rate of 60 cm/min. The coated electrodes were then heated in air at 120 °C for 15 min. All Ir electrodes were oxidized to hydrous IrOx by potential cycling between −0.8 V and 0.9 V in pH 7 phosphate buffer solution, similar to the potential range used by Silva et al. [47].

2.2. Electrochemical Equipment

Most of the electrochemical experiments were carried out using an AUTOLAB system equipped with a standard PC

computer. In some experiments, an EG&G Parc 173 potentiostat with an EG&G Parc 175 function generator were used, and a Kipp & Zonen (Mandel Scientific Co. Ltd.) or LY-14100-II (Linseis) X-Y recorder were used to record the electrochemical data.

2.3. Solutions, Reagents and General Experimental Conditions

All solutions were prepared using A.C.S. analytical grade chemicals and triply distilled water. H_2O_2 (30% v/v aqueous solution), D-glucose and potassium dihydrogen phosphate were purchased from BDH Chemicals. Glucose oxidase (GOx, type II-S from *Aspergillus niger*, 40,300 unit/gram of solid) was obtained from Sigma. All experiments were carried out in aerated pH 7 phosphate buffer solutions at room temperature.

2.4. GOx Immobilization in Ir Oxide Films

Immobilization of GOx was achieved by immersion of an Ir electrode (Ir wire or Ir sputtered on glass plates) in a concentrated solution of GOx (4000 U/mL) for 5 min, followed by IrOx growth by potential cycling in a pH 7 phosphate buffer [Method A, [34]]. This procedure was repeated several times, alternately growing more IrOx film and depositing more GOx up to 20 monolayers of IrOx film. (Method A [34]).

2.5. STM Imaging

Scanning Tunneling Microscopy (STM) images of SG-derived Ir nanoparticles, deposited on sputtered Au surfaces, were collected at ambient conditions using a Digital Instruments Nanoscope II. All images were obtained in the constant current mode using commercial (DI) or mechanically cut Pt/Ir tips. Images from 1 μm × 1 μm down to 20 nm × 20 nm were typically obtained for each surface examined.

3. Results and Discussion

3.1. Growth and Relevant Properties of Hydrous Ir Oxide Electrodes on Ir (Ir/IrOx)

Hydrous IrOx films can be formed electrochemically on Ir metal substrates (Ir wires, foils, and sputtered Ir coatings) in a pH 7 phosphate buffer solution by cycling over a wide potential range, encompassing the evolution of both oxygen and hydrogen. After a few minutes of cycling between −0.8 V and 0.9 V (curves (- - - -) and (-·-·-·) in Fig. 1A), anodic peaks at 0.12 V (A_1) and 0.50 V (A_2) and cathodic peaks at 0.08 V (C_1) and 0.45 V (C_2) are seen to develop, reflecting the Ir(III)/Ir(IV) and Ir(IV)/Ir(V,VI) redox

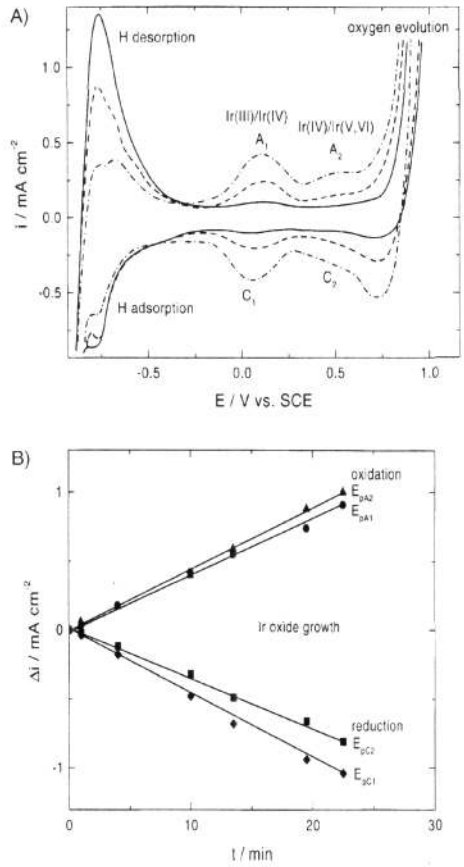

Fig. 1. A) Cyclic voltammetric response (0.1 V/s) of Ir wire (——) and IrOx formed electrochemically on Ir wire by cycling the potential between −0.8 V and 0.9 V (vs. SCE) in pH 7 phosphate buffer solution. The IrOx film thickness, given in monolayers, increases with time of cycling: (- - - -) 2 and (-·-·-·) 4 monolayers. B) IrOx current densities, Δi (corrected for the background current at Ir metal) vs. various times of growth at 0.1 V/s in pH 7 phosphate buffer solution. Currents given at CV peak potentials: $E_{pA1} = 0.12$ V, Ir(III)/Ir(IV); $E_{pA2} = 0.5$ V, Ir(IV)/Ir(V,VI); $E_{pC1} = 0.08$ V, Ir(IV)/Ir(III) and $E_{pC2} = 0.45$ V, Ir(V,VI)/Ir(IV).

reactions within the IrOx oxide film. As calculated from the total charge passed in slow sweep rate CVs (up to 0.65 V), the thickness of the two oxide films in Figure 1A is equivalent to 2 and 4 monolayers, respectively (0.11 mC/cm^2/monolayer, [52, 53]). With continued cycling, these peaks can be increased further in size as the film thickens, from few monolayers up to a maximum of several micrometers in thickness [42, 43]. On sputtered Ir coatings, the thickness of the IrOx film will be limited by the thickness of the underlying Ir layer, normally only ca. 200 nanometers in thickness.

IrOx films are conductive in the oxidized (IV, V, VI) forms and non-conductive in the reduced (III) state [39]. Further growth of the hydrous oxide can be prevented in the phosphate buffer solution by restricting the potential limits to within −0.7 to +0.75 V. Once formed, the oxide cannot

be reduced back to the metal in aqueous solutions [42, 43]. In fact, the oxidation of Ir metal and the growth of an IrOx film are difficult to avoid. To preserve a metallic Ir surface, the positive potential limit during cycling cannot exceed 0.4 V (vs. SCE) [67]. These characteristics are quite different from those at metals such as Pt, Pd and Au [68–70], at which only thin, compact oxide films can be formed in the same potential range as employed in Figure 1A. Hydrous oxide films can also be made to deposit at these other metals by multi-cycling techniques, but much higher potentials are required to achieve this. Also, the resulting hydrous oxide films are non-conducting in nature and can be fully reduced in the negative scan, contrary to the case for IrOx films.

The hydrogen adsorption/desorption (H upd) peaks, which are characteristic of metallic Ir exposed to an aqueous solution, are seen for the IrOx electrode in the potential range from ca. −0.4 V to ca. −0.75 V. In Figure 1A, the focus should be on the cathodic H peak, which, as expected, is seen to decrease somewhat in size as the IrOx film is formed. The anodic H peak in the first CV cycle also includes hydrogen gas oxidation, thus explaining its large size. The fact that the H upd peaks remain visible in the CV, despite the presence of an overlying IrOx film, has been attributed [40] to the porous nature of the oxide structure, which allows for the transport of hydrogen ions to and from the underlying Ir surface. The oxygen reduction reaction has a relatively low activity at Ir/IrOx electrodes, especially as compared to the activity seen at Pt, and thus only a small negative offset to the Ir/IrOx CV (negative of −0.2 V) is seen in Figure 1A in the presence of oxygen.

The IrOx redox reactions are rapid [43, 45, 46]. Indeed, the IrOx redox peaks increase linearly with sweep rate (up to at least 0.2 V/s) for thin films of at least 50 monolayers in thickness [45, 46], reflecting reversible redox conditions. This reversible response is seen even for much thicker oxides, consisting of hundreds of monolayers, due to the rapid transport of electrons and ions through the hydrous oxide material [45, 46].

The rate and extent of growth of the IrOx film can be monitored, either oxidatively or reductively, at any potential within the range of its redox activity (−0.1 V to 0.55 V). Figure 1B demonstrates the rate of oxide growth by tracking the current at the four peaks in the CV in Figure 1A, both during oxidation (0.12 V for A_1 and 0.50 V for A_2) and reduction (0.08 V for C_1 and 0.45 V for C_2). The peak currents, corrected for the background currents at bare Ir observed when no hydrous oxide is present, are plotted in Figure 1B as Δi versus the time of potential cycling (t) at 0.1 V/s. The slightly different slopes in Figure 1B for the four peaks is due to the small differences in the size of the four IrOx CV peaks, as seen in Figure 1A.

As shown in our previous papers [45, 46], due to the uniformity of the IrOx structure, the monitoring of Ir oxide growth can be accomplished not only by measuring the charge passed, but also directly from the peak current, thus simplifying the data treatment. The growth rate of IrOx films is relatively slow in pH 7 phosphate buffer solution [34], as compared to the more typically employed sulfuric acid solution [42, 45–47, 52, 53]. For example, to obtain the equivalent of four monolayers of IrOx, as in the largest CV in Figure 1A, 10 minutes of potential cycling is required in phosphate buffer solution (Fig. 1B), while in H_2SO_4 solutions, only 2 minutes yield a film of comparable thickness [53]. This relatively slow growth of the oxide may be beneficial, however, to allow for sufficient time for the simultaneous incorporation of an enzyme into the oxide structure [34].

The stability of the Ir/IrOx electrode is remarkable. It can be stored in the dry state for months [38–47] and the electrochemical response can then be fully restored within a few potential cycles. Its high stability, corrosion resistance [47, 49], and biocompatibility [50] allow for the application of Ir/IrOx electrodes in pH [55–57] and NO detection [61], particularly for in vivo neural stimulation [49, 50], for urea [58, 59] and ascorbic acid [60] detection, and, more recently, as a glucose biosensor [33, 34].

3.2. Detection of H_2O_2 at Ir/IrOx Electrodes

3.2.1. Enhanced IrOx Film Growth at Low H_2O_2 Concentrations

At Ir and Ir/IrOx electrodes, an unusual effect is observed in the presence of micromolar concentrations of H_2O_2, allowing for the detection of low concentrations of H_2O_2 by the enhanced growth of an IrOx film and hence an increase in the IrOx CV response. To demonstrate this, Figure 2A (inner solid curve) depicts the CV response of an IrOx coating, formed electrochemically on an Ir sputter-coated glass electrode by cycling at 0.1 V/s between −0.8 V and 1.2 V. Further growth of the IrOx film was prevented by limiting the negative potential limit to −0.7 V and the positive limit to 0.8 V. The electrochemical response of this electrode is seen to be similar to that of an IrOx film formed on an Ir wire (Fig. 1A).

Interestingly, when micromolar additions of H_2O_2 are then introduced to the buffer solution, the entire IrOx CV profile increases in magnitude, similar to what would be expected if the IrOx film had been thickened by cycling over the wider potential window normally employed for oxide growth. These increased currents, at all potentials positive of −0.25 V (Fig. 2A), would also be seen if the roughness of the electrode had increased in the presence of H_2O_2. However, the change in the roughness factor of the electrode cannot be significant, since the hydrogen adsorption/desorption peaks, used for determining the real surface area of the electrode, remain essentially unchanged with the addition of these small concentrations of H_2O_2.

Figure 2B shows the dependence of the CV peak currents (at 0.1 V/s) of an IrOx film, formed as shown in Figure 2A (catalytic growth), on the incremental additions of 1.2 μM H_2O_2, up to 8.4 μM, at A_1(0.12 V), A_2 (0.5 V), C_1 (0.08 V) and C_2 (0.45 V). Importantly, a linear dependence on the H_2O_2 concentration, even at these very low concentrations is seen. (Note that micromolar levels of H_2O_2 cannot be

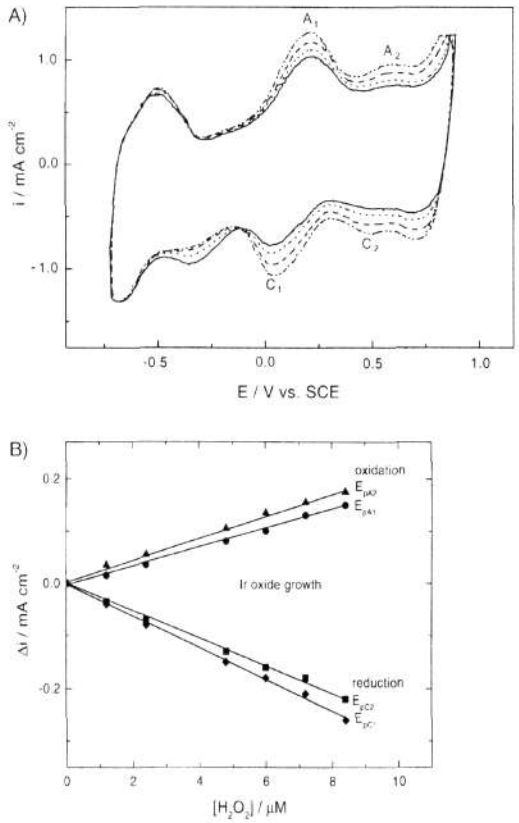

Fig. 2. A) Cyclic voltammetric response (0.1 V/s) in pH 7 phosphate buffer solution of Ir oxide, formed on sputtered Ir, to the incremental additions of H_2O_2: (——) 0 μM, (·····) 2.4 μM, (- - - -) 4.8 μM, (–··–) 6.0 μM. B) IrOx currents densities, Δi (corrected for background current in the absence of H_2O_2), vs. H_2O_2 concentration in pH 7 phosphate buffer solution (0.1 V/s) at peak potentials: $E_{pA1} = 0.12$ V, Ir(III)/Ir(IV); $E_{pA2} = 0.5$ V, Ir(IV)/Ir(V,VI); $E_{pC1} = 0.08$ V, Ir(IV)/Ir(III) and $E_{pC2} = 0.45$ V, Ir(V,VI)/Ir(IV).

detected via the oxidative or reductive route (see section 3.2.2.)). The detection of micromolar quantities of H_2O_2 by tracking the increase in the IrOx redox peaks could be of interest for application in newly developed transdermal devices used for the detection of glucose [2,3] and in the detection of H_2O_2 produced in leukocytes [4]. Also, the detection of H_2O_2 through the enhancement of the IrOx CV signal (Fig. 2A), instead of via the more typical direct oxidative or reductive detection of H_2O_2 (section 3.2.2), as at Pt, could be advantageous in terms of sensor specificity and stability.

The ability to monitor the H_2O_2 concentration over a wide range of potentials, (−0.1 V to 0.75 V), is particularly beneficial in overcoming potential-dependent interferences from oxygen or other redox active species. Oxygen reduction at IrOx electrodes is seen only as a small cathodic current at potentials negative of −0.2 V (see section 3.1). This broad potential window for H_2O_2 detection results in greater sensor flexibility, in that any potential within this range can be selected to fit a desired application and avoid particular interferences. Also, the observed high current densities, in the range of 0.1 to 0.3 mA/cm², vs. μA/cm² (Fig. 2), are advantageous, allowing miniaturized, screen-printed [54] Ir/IrOx electrodes to operate at relatively high current ranges.

The origin of the enhanced growth of IrOx in the presence of H_2O_2, without extending the upper potential limit to the normally required values, is not yet understood. However, it may be related to the generation of hydroxyl radicals, formed in the Fenton reaction, normally involving Fe(II) (depicted as M) ions in solution [64].

$$M(II) + H_2O_2 = M(III) + OH^{\cdot} + OH^- \quad (1)$$

By analogy, H_2O_2 could react with the Ir(III) or Ir(IV) sites in the IrOx film, oxidizing them to a higher oxidation state in a reaction in which hydroxyl radicals and OH^- ions are produced. The higher pH generated within the film could result in the Ir sites within IrOx being subjected to a higher real potential, such that additional hydrous IrOx film could then be formed. Alternatively, the hydroxyl radicals may react directly with the compact IrOx film underlying the hydrous oxide, causing new IrOx to form, similar to what is normally achieved by cycling to high potentials. This latter explanation would be in agreement with reports of IrOx formation via the irradiation of Ir salt solutions, resulting in the production of hydroxyl radicals [65].

3.2.2. *Detection of Higher Concentrations of H_2O_2 by its Oxidation/Reduction on Ir, Ir/IrOx and Ir/IrOx-GOx Electrodes*

At H_2O_2 concentrations greater than 0.1 mM, the enhanced IrOx CV signal, shown in Figs. 1 and 2, is no longer seen, and the mode of detection of H_2O_2 prevailing now is via its reduction and oxidation, as has also been reported for Pt [5–11] and other metallic [12–17] or metallized [20] electrodes. Figure 3 demonstrates the reduction and oxidation of 2 and 4 mM H_2O_2 on metallic Ir in a pH 7 phosphate buffer solution. To avoid Ir metal oxidation, the positive potential limit of the scan was limited to 0.45 V in this experiment [40, 42].

The reduction of H_2O_2 on Ir metal is seen either as just a wave or as a wave and a peak (Fig. 3), with a half-wave potential, $E_{1/2}$, for the first wave located at ca. −0.10 V, more negative than at bare Pt (Table 1). This indicates a higher overpotential and therefore slower reaction kinetics of this reaction on Ir vs. Pt. This overpotential demonstrates that Pt is a better H_2O_2 reduction catalyst than is metallic Ir. The oxidation of H_2O_2 also occurs at a higher overpotential at Ir (Fig. 3) vs Pt, since a well-developed oxidation current plateau is not seen for Ir in Figure 3 and as the H_2O_2 oxidation currents at Ir are much smaller than those for H_2O_2 reduction. The slower oxidation kinetics at metallic Ir vs. Pt correlates with the fact that Ir is likely already covered with a thin compact oxide at ca. −0.5 V (vs. SCE), while for

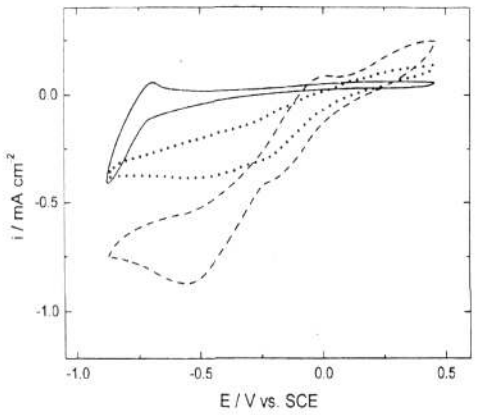

Fig. 3. Cyclic voltammetric response of Ir wire in pH 7 phosphate buffer solution in (——) 0 mM, (·····) 2 mM and (- - - -) 4 mM H_2O_2.

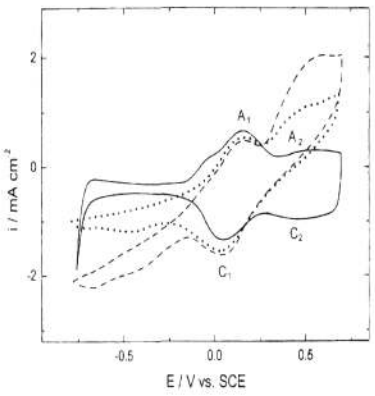

Fig. 4. Cyclic voltammetric response of Ir/IrOx electrode in pH 7 phosphate buffer solution in (——) 0 mM, (·····) 8 mM and (- - - -) 12.5 mM H_2O_2.

Pt, the oxide is not formed until potentials greater than 0.1 V [43]. Increasing the upper limit of the scan to 0.6 V (not shown in Fig. 3) yields a further increase in the H_2O_2 oxidation currents on metallic Ir, although even then, a true current plateau is not reached, indicative of the relative slowness of the reaction. Similarly, a significant increase in the currents due to the oxidation of H_2O_2 on electroplated Ir electrodes is seen [27] only when the potential is extended quite positively.

At IrOx films formed electrochemically on Ir wire electrodes (Fig. 4), the half-wave potential for the H_2O_2 reduction reaction is difficult to determine, due to the overlap with the IrOx reduction peak. However, the reaction is underway already at 0.10 V, as seen by the increased cathodic currents at the C_1 peak. Also, the half-wave potential, determined after subtraction of the background IrOx current, is close to −0.10 V (Table 1), i.e., similar to the $E_{1/2}$ value for bare Ir. The H_2O_2 reduction

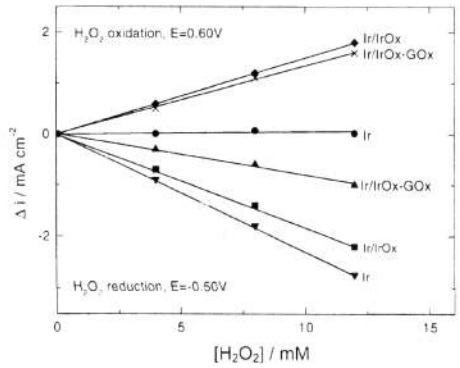

Fig. 5. H_2O_2 oxidation ($E = 0.5$ V) and reduction ($E = -0.5$ V) current densities, Δi, corrected for the background currents in the absence of H_2O_2, at Ir/IrOx and Ir/IrOx-GOx electrodes in pH 7 phosphate buffer containing 8 mM H_2O_2. Oxidation potential for Ir metal is 0.4 V and reduction −0.5 V (see text).

current plateau on Ir/IrOx is reached at −0.25 V and −0.5 V for 4 mM and 8 mM H_2O_2, respectively, similar to what is seen at Ir (Fig. 3). In contrast, it can be clearly seen that the oxidation of H_2O_2 (Fig. 4) occurs at a significantly lower overpotential and is therefore more rapid at Ir/IrOx electrodes vs. at metallic Ir (note again that a compact Ir oxide film will be present on metallic Ir in this potential range). Now, the H_2O_2 oxidation currents are very similar in magnitude to the reduction currents (Fig. 4).

Figure 5 summarizes the measured reduction (at −0.5 V) and oxidation (at 0.6 V) current densities, Δi, corrected for the background current in the absence of H_2O_2, to incremental additions of H_2O_2 at metallic Ir wire electrodes, at Ir/IrOx and at Ir/IrOx-GOx electrodes, the latter referring to an IrOx film formed electrochemically on Ir wire electrodes in the presence of GOx [34]. In terms of H_2O_2 reduction, the measured currents are slightly lower at Ir/IrOx vs. at Ir, likely as the Ir surface is covered by the non-conducting, porous IrOx film at this potential, so the available active area is lowered. For the Ir/IrOx-GOx electrode, a significant lowering of the H_2O_2 reduction current densities, by ca. 2.5 times (Fig. 5), is observed, as compared to IrOx alone. This decrease may be due to blocking of the pores in the IrOx film by the enzyme, even though the enzyme has been added to the solution after IrOx growth has already been initiated [34] (see Sec. 2).

The reductive detection of H_2O_2 on metallic Ir (at −0.1 V vs. Ag/AgCl) has been used [27] in a glucose biosensor consisting of a carbon fiber microelectrode, coated with co-deposited Ir metal and GOx (Ir/GOx-carbon fiber electrode), but the linear range of glucose detection was limited to only a few mM. With the use of reductive H_2O_2 detection, the oxidation of interfering species can be avoided, but the reduction signal (Figure 3) at Ir metal or IrOx electrodes (Figure 4) is often difficult to evaluate, as it sometimes forms as two waves or as a wave and a peak. As a result, the measured currents may depend significantly on the detection potential employed.

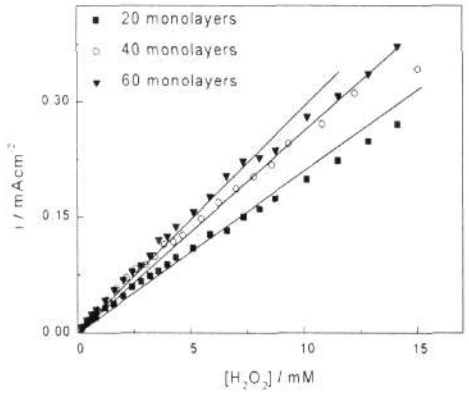

Fig. 6. Chronoampermetric data collected at 0.55 V for three different IrOx films formed electrochemically at Ir-sputtered glass plate during the incremental addition of H_2O_2 to stirred phosphate buffere solution (pH 7).

As stated above, a significant increase in the H_2O_2 oxidation current density is seen (Figure 5) at the hydrous Ir/IrOx electrode vs. at Ir. The Δi values at 0.6 V, i.e., within the oxidation plateau, are much higher for this particular IrOx film as compared to bare Ir, even though the onset of H_2O_2 oxidation is seen at ca. 0.15 V at both electrodes (Figs. 3 and 4). This result points to the important role of the IrOx film in the oxidation of H_2O_2, and indicates clearly that H_2O_2 oxidation occurs predominantly at the IrOx surface vs. at the underlying Ir substrate. Indeed, the measured H_2O_2 oxidation currents have been found to be affected by the film thickness of IrOx, as shown in Figure 6. This is beneficial from the point of view of sensor development. If H_2O_2 oxidation occurred on the underlying Ir surface, then the response should deteriorate with increasing film thickness, as the underlying Ir would become increasingly less accessible. However, the opposite effect is observed.

Figure 6 shows a set of chronoamperometric data collected at 0.55 V for H_2O_2 oxidation at IrOx films of three different film thicknesses. Figure 6 shows that, up to at least 10 mM, the current density is linearly proportional to the H_2O_2 concentration, indicating that the system is predominantly diffusion controlled under these conditions for these three films.

However, at higher concentrations, this linearity is no longer observed, and at even higher concentrations (not shown), the current densities begin to develop a plateau, similar to what would be expected for Michaelis-Menten kinetics. The apparent Michaelis-Menten constants (K_m') for the three curves in Figure 6 are 11, 14 and 16 mM, increasing with an increase in IrOx film thickness. Analogous to what was reported by Hall et al. [12] for H_2O_2 oxidation at Pt, this behavior may indicate the adsorption of H_2O_2 on the IrOx surface. This is also consistent with the fact that Figure 6 shows an increase in current density with increasing film thickness (increasing number of IrOx sites). The fact that the current densities are not linearly proportional to the film thickness likely indicates that not all of the sites within the IrOx film are accessible to H_2O_2, and thus cannot be utilized.

The H_2O_2 oxidation mechanism at hydrous IrOx films may involve a redox mediation mechanism:

$$Ir_2O_5 \cdot nH_2O + H_2O_2 \rightarrow Ir_2O_4 + (n+1)H_2O + O_2 \quad (2)$$

$$Ir_2O_4 + (n+1)H_2O \rightarrow Ir_2O_5 \cdot nH_2O + 2ne^- + 2nH^+ \quad (3)$$

with the overall net reaction being:

$$H_2O_2 \rightarrow 2H^+ + O_2 + 2e \quad (4)$$

Ir(V) (and Ir(VI)) sites, stable at 0.6 V, are reduced to Ir(IV) by hydrogen peroxide and then are oxidized electrochemically back to Ir(V,VI) at the detection potential employed, resulting in the catalytic oxidation of H_2O_2. This is consistent with a previous report in alkaline solutions, in which H_2O_2 oxidation on IrOx, formed by sputter-coating carbon, commences only at potentials at which the Ir(V,VI) states are generated. As well, Mn oxide [31] and the + V/VI states of W oxide [35, 36], deposited on GC electrodes have been considered as mediators for H_2O_2 oxidation in the past.

On Pt, a linear current response can be obtained only up to 1 mM H_2O_2 [10]. However, in the case of the IrOx electrodes under study here, Figure 5 shows that the response is linear up to at least 12 mM. This is consistent with earlier reports [37] for IrOx films formed on Ir wires, in which the response to increasing H_2O_2 concentrations in 1 M KCl is linear up to 10 mM, while it is as high as 20 mM for IrOx films formed on Ir metal electrodeposited on glassy carbon electrodes.

3.3. Effect of Substrate (S) on Response of S/IrOx to H_2O_2

3.3.1. Formation and Characteristics of S/IrOx Films

In the previous section, it has been argued that the reduction of H_2O_2 at Ir/IrOx electrodes occurs at the underlying Ir metal substrates, based on the similarity of the measured currents at bare vs. IrOx-covered electrodes (Fig. 5). In contrast, H_2O_2 oxidation is much more rapid on the IrOx vs. Ir surface, suggesting that on Ir/IrOx, this reaction occurs preferentially on the oxide surface. In order to test these suggestions, IrOx films have been deposited on a range of substrates (Pt, Ir and glassy carbon (GC)) of differing catalytic impact on H_2O_2 oxidation and reduction. It is then predicted that the H_2O_2 reduction rates should depend on the nature of the substrate, while H_2O_2 oxidation should not.

As shown in our prior work [52, 53], Ir metal can be deposited as a sol, resulting in thin films composed of metallic Ir nanoparticles, 2–3 nm in diameter, as seen in TEM images [53]. Figure 7A shows an STM image of the resulting Ir sol on a sputtered Au surface (on glass). These images confirm that Ir nanoparticles are indeed formed, in this case, being ca. 3 nm in diameter. It was shown that these Ir nanoparticles can be oxidized to IrOx [52], using the same potential cycling regime as for Ir wire substrates (Fig. 1).

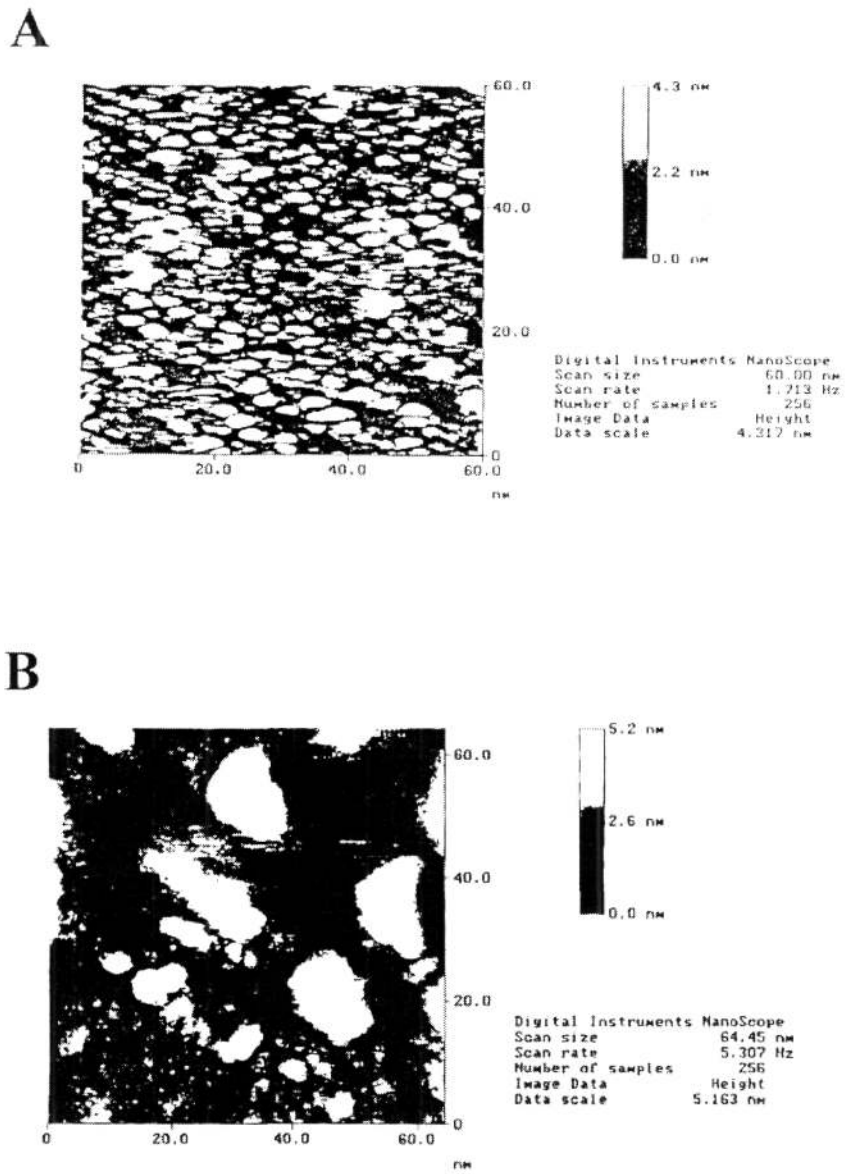

Fig. 7. A) STM image of nanoparticulate Ir sol, dip-coated on Au-sputtered glass plate using constant withdrawal rate of 60 cm/min and then dried at 120 °C for 15 min. B) STM image of nanoparticulate Ir sol (e.g., Fig. 7A) after electrochemical conversion to IrOx.

However, contrary to the case at bulk Ir, IrOx formation is complete within a few potential cycles, i.e., no further IrOx growth by potential cycling is possible [52]. This implies that all of the nanoparticulate Ir has been converted to IrOx, confirmed by the complete disappearance of the H-peaks, which are characteristic of metallic Ir. Figure 7B shows an STM image of the Ir sol coating after complete electrochemical oxidation to IrOx. It can clearly be seen that some of the nanoparticles have now fused together and become larger, forming particles 20–30 nm in diameter. This increase in size of these particles is consistent with the much lower density of hydrous IrOx [42] and the resulting electrode can therefore now be described as Au/IrOx.

In the present work, two electrode materials, Pt and GC, were selected to establish the impact of the IrOx substrate on the H_2O_2 reactions. These were chosen for its known significantly different [62, 63] catalytic impact on H_2O_2 redox reactions. Figure 8 shows the cyclic voltammograms of IrOx films, formed by the complete electrochemical conversion of Ir sols which were deposited in an identical fashion on Pt (solid line) and GC (dashed line), forming Pt/IrOx and GC/IrOx electrodes, respectively. As expected, no

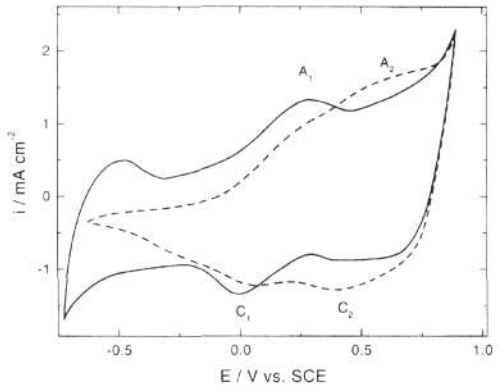

Fig. 8. Cyclic voltammetric response (0.1 V/s) in pH 7 phosphate buffer solution of nanoparticulate IrOx on sputtered Pt (——) and (- - - -) GC substrates.

hydrogen adsorption/desorption (upd) peaks are seen for GC/IrOx at negative potentials, while for Pt/IrOx, these peaks are clearly present, reflecting the varying abilities of these substrates to adsorb hydrogen. While the magnitude of the IrOx redox peaks are very similar in the two cases, their potentials are somewhat different, showing a larger peak separation, i.e., slower IrOx redox reactions in the case of GC/IrOx.

3.3.2. H_2O_2 Reduction at S/IrOx films

Figure 9 shows the cyclic voltammetry response of these S/IrOx electrodes to H_2O_2 just in the range of potential of H_2O_2 oxidation/reduction. For bare sputter-coated Pt ((a) of Fig. 9A), H_2O_2 reduction commences at ca. +0.2 V, reaching a plateau at ca. −0.3 V. The $E_{1/2}$ value is ca. 0.15 V (Table 1), in agreement with the literature data [63] at a polycrystalline Pt foil electrode. For the Pt/IrOx film, Figure 9A (b) shows that the currents due to IrOx reduction, H deposition on Pt, and H_2O_2 reduction all overlap, leading to uncertainty in the potential of onset of H_2O_2 reduction and in the value of the background current, and consequently, in the $E_{1/2}$ value for this reaction. From the raw data, the $E_{1/2}$ value for H_2O_2 reduction at Pt/IrOx can be seen to be more positive than 0.0 V. However, when the CV response in the absence of H_2O_2 is subtracted from the H_2O_2 runs, the estimated $E_{1/2}$ value is ca. +0.05 V, closer to the value for bare Pt (Table 1). Note that the H upd peaks are altered somewhat in the presence of H_2O_2 (Fig. 9), thus making the selection of the correct baseline difficult and possibly introducing some error into the $E_{1/2}$ value.

On bare GC (Fig. 9B, a), the H_2O_2 reduction reaction is clearly kinetically much slower than at Pt and is seen to commence only when the potential is extended negatively to −0.1 V, ca. 0.3 V more negative than on Pt. Also, a current plateau is never reached, even when the potential is scanned to −0.65 V (Table 1). At GC/IrOx (Fig. 9B), when the currents in the absence of H_2O_2 are subtracted from those at various H_2O_2 concentrations, the $E_{1/2}$ value (Table 1) is still

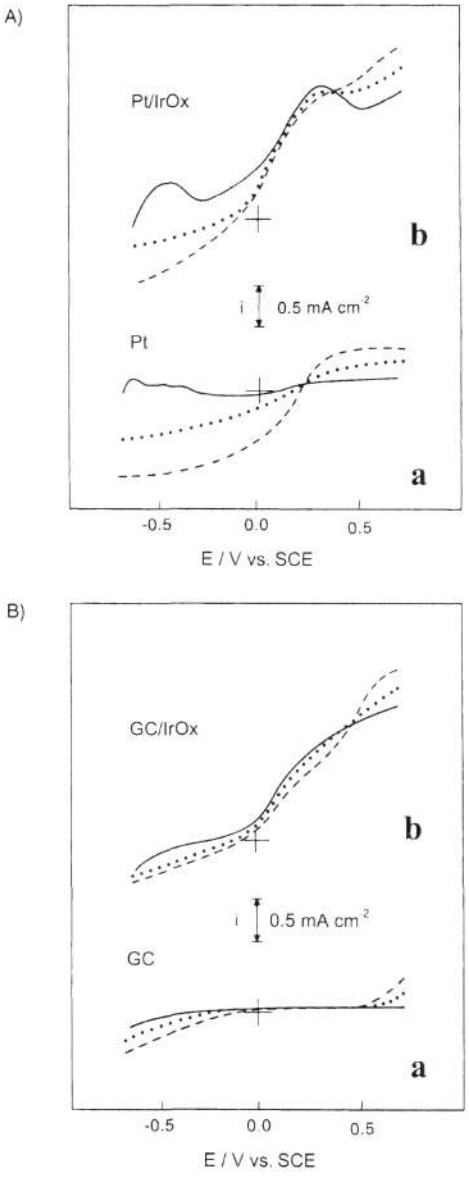

Fig. 9. A) Cyclic voltammetric responses of Pt and Pt/IrOx electrodes in pH 7 phosphate buffer at various concentrations of H_2O_2: (——) 0 mM, (·····) 4 mM and (- - - -) 8 mM. B) Cyclic voltammetric responses of GC and GC/IrOx electrodes in pH 7 phosphate buffer at various concentrations of H_2O_2: (——) 0 mM, (·····) 4 mM and (- - - -) 8 mM.

seen to be more negative than −0.65 V ($E_{1/2} \approx -0.7$ V [63]). For the Ir/IrOx electrode (Fig. 4), the $E_{1/2}$ for H_2O_2 reduction (after subtraction of the IrOx background currents) is close to the value observed for bare Ir (ca. −0.1 V, Table 1). The fact that, due to kinetic limitations, the redox reactions of H_2O_2 on GC occur at high overpotentials has been used recently [66] in a reagentless glucose sensor based on GOx entrapped into osmium complex modified poly-

Table 1. Half-wave potentials for H_2O_2 reduction and oxidation on IrOx formed electrochemically on Ir wire and on Ir sol on various substrates (S).

Electrodes	$E_{1/2}$ (V) vs. SCE at 0.1 V/s, 0.1 M phosphate buffer pH 7			
	Oxidation		Reduction	
	Literature	This work	Literature	This work
Bare electrodes				
Ir	> 0.3 [27]	> 0.25	< − 0.1 [27]	− 0.10
Pt	0.19 [62]	0.25	0.15 [62]	0.15
GC	0.70 [62]	> 0.65	< − 0.65 [62]	< − 0.65
IrOx on Ir wire	–	0.35	–	ca. − 0.10
(S)/IrOx on Ir sol				
Ir/IrOx	–	0.55	–	ca. − 0.10
Pt/IrOx	–	0.55	–	ca. 0.05
GC/IrOx	–	0.55	–	< − 0.65

Table 2. Response to H_2O_2 (oxidation and reduction up to 10 mM)) on IrOx formed electrochemically on Ir wire and on Ir sol on various substrates (S).

Electrode	Sensitivity ($\mu A\ mM^{-1}\ cm^{-2}$), pH 7, 0.1 M phosphate buffer			
	Oxidation		Reduction	
	$E = 0.55$ V	$E = 0.65$ V	$E = -0.1$ V	$E = -0.2$ V
Bare electrodes				
Ir	25 [a]	25 [a]	100	125
Pt	135	135	260	300
GC	2	75	10	35
IrOx on Ir wire	150	150	45	75
(S)/IrOx on Ir sol				
Ir/IrOx	90	185	50	90
Pt/IrOx	100	200	155	190
GC/IrOx	90	175	15	40

[a] Ir covered by compact oxide film at these potentials.

(pyrrole) films to prevent co-oxidation of enzymatically generated H_2O_2 in the presence of molecular oxygen.

The role of the substrate and lack of impact of the IrOx film on the reductive detection of H_2O_2 is also clearly seen when the current sensitivities (in $\mu A\ mM^{-1}\ cm^{-2}$) for the bare substrates (S = Pt, Ir and GC) are compared with the S/IrOx electrodes in Table 2. The potentials chosen for comparison are − 0.1 V and − 0.2 V, sufficiently positive to avoid interference with the H adsorption currents during the measurement of the background current in the absence of H_2O_2. Much higher currents are observed (after subtraction of the baseline data in the absence of H_2O_2) for Pt/IrOx electrodes at − 0.1 and − 0.2 V, respectively, than for the corresponding GC/IrOx electrodes at the same potentials. Also, the sensitivity of Ir/IrOx electrodes is notably greater than at GC/IrOx.

These data do strongly suggest that H_2O_2 reduction proceeds at a rate consistent with the properties of the underlying electrode substrate and that the hydrous IrOx films do not promote H_2O_2 reduction. The porous structure of the hydrous oxide appears to allow for the penetration of H_2O_2 into the oxide film, as seen in Figure 6, and for the reduction process to occur at the S/IrOx interface, as expected, based on the low conductivity of the reduced form of IrOx [39].

3.3.3. *H_2O_2 Oxidation at S/IrOx Films*

As H_2O_2 oxidation occurs at a potential at which the conducting Ir(IV) form of IrOx is stable, the film would be expected to play a significant role in H_2O_2 oxidation and the nature of the substrate should not notably influence the H_2O_2 oxidation kinetics. On bare Pt and GC (Fig. 9), the $E_{1/2}$ values for H_2O_2 oxidation are 0.25 V and > 0.65 V, respectively, close to the values reported in previous work (0.19 V and 0.7 V, [62]). For the IrOx coated substrates, Figure 9 shows that the H_2O_2 oxidation waves at both Pt/IrOx and GC/IrOx overlap with the IrOx peaks. Even so, the $E_{1/2}$ values, which can be more accurately estimated than for H_2O_2 reduction, are very similar for these two substrates (and for SG-derived IrOx on Ir), i.e., 0.55 V (Table 1), but very different from the values at the bare electrodes. These results show that the effect of the substrate material beneath the IrOx film on the H_2O_2 oxidation kinetics is minimal or non-existent, as would be expected based on the excellent IrOx conductivity at these potentials.

More evidence for the importance of IrOx in the oxidative detection of H_2O_2 can be gained from a comparison of the current sensitivities for H_2O_2 oxidation on the bare substrates vs. at S/IrOx electrodes. The currents have been corrected for the background signal in the absence of H_2O_2 (see Fig. 9) and are taken at the half-wave potentials (0.55 V) and in the plateau region (0.65 V) of the oxidation waves at S/IrOx electrodes. At these potentials, a current plateau would be expected for bare Pt (Fig. 9A), while only a small increase in the current at bare GC would be seen (Fig. 9B). Instead, the sensitivity at all of the IrOx coated substrates is similar, within experimental error (Table 2). This again supports our previous conclusion that IrOx plays a major role in the oxidation of H_2O_2.

The significant difference between the response of Pt and GC electrodes to H_2O_2 oxidation has been used in previous work [63] to assess the mediating abilities of ruthenium poly(pyridine) complexes, e.g., $[(2.2'bpy)_2(OH)Ru^{III}ORu^{III}(OH)(2.2'bpy)_2]^{4+}$, employed in a 'second generation' biosensor. These sensors have been formed by the immobilization of these complexes in a β-polycyclodextrin polymer containing GOx, followed by deposition on Pt or GC. These glucose biosensors respond to the glucose concentration either at the potential of the mediator, when it oxidizes the enzyme, or at the potential typical for H_2O_2 oxidation directly on the Pt or GC substrate. This latter situation occurs if, instead of the mediator, oxygen oxidizes the enzyme, producing H_2O_2. For a highly efficient mediator, the $E_{1/2}$ value associated with the oxidative response to glucose is independent of the substrate material employed, as seen for Pt (0.19 V) and GC (0.20 V). These values correlate well with the redox potential of the mediator (0.24 V). For less efficient mediators, e.g., $[Ru^{II}(trpy)(phen)(OH_2)]^{2+}$, having a redox potential 0.4 V, the $E_{1/2}$ values do then depend on the substrate employed, e.g., 0.25 – 0.30 V for Pt and 0.45 – 0.50 V for GC. These results indicate that the oxidation of the mediator and of H_2O_2 occur simultaneously on the electrode, with a preference for H_2O_2 oxidation when the underlying electrode substrate is Pt vs. GC. Another example [62] of the use of GC, instead of Pt, in monitoring the response of a reagentless glucose sensor, is based on glucose oxidase entrapped in osmium complex-modified poly(pyrrole) films to prevent the concurrent oxidation of enzymatically generated H_2O_2 in the presence of oxygen.

4. Ir/IrOx Based Glucose Biosensor

The conclusions drawn from studying the response of Ir metal and IrOx electrodes to H_2O_2 can be used to optimize the operating conditions of biosensors based on IrOx electrodes. Considering that the oxidation of common interfering substances (ascorbate, paracetamol, urea [34]), at their physiological concentrations, does not occur at any measurable rate at IrOx, the oxidative detection of H_2O_2 is preferable over the reductive mode of H_2O_2 detection. This is for the following reasons: a) interference from oxygen reduction is not an issue (Fig. 4), b) a linear response up to ca. 12 mM (Fig. 5) and ca. 10 mM H_2O_2 (Fig. 6) is obtained, c) the oxidative response depends partially on the IrOx film thickness, and d) the response is very similar, even with the immobilization of GOx in the IrOx film (Fig. 5). Indeed, Figure 10 shows that an excellent response to glucose, based on the catalytic growth effect mentioned earlier (section 3.2.1) at $E_{pA1} = 0.12$ V, can be seen up to at least 40 mM glucose when using a Ir/IrOx-GOx electrode at low GOx loading.

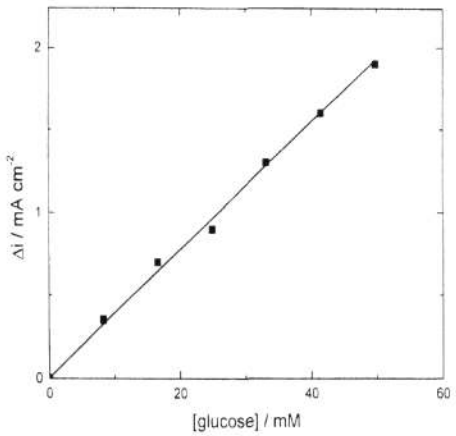

Fig. 10. Response of Ir/IrOx-GOx electrode formed on Ir sol to glucose in an unstirred pH 7 phosphate buffer solution at 0.12 V.

A linear dependence of the H_2O_2 oxidation currents at 0.60 V on the H_2O_2 concentration is seen in Figure 5 up to 12 mM H_2O_2 for hydrous IrOx electrodes, e.g., for Ir/IrOx-GOx and also without the incorporated enzyme. The operating linear range is, in fact, wider than this. In previous work [34], we have reported a linear dependence of the H_2O_2 oxidation current densities, measured at 0.35 V (1.2 V vs. RHE), on concentrations up to ca. 20 mM H_2O_2 for Ir/IrOx films.

5. Conclusions

Ir oxide electrodes are promising materials for H_2O_2 sensing, due to their high stability, biocompatibility, insensitivity to common interfering substances, unchanging response at constant potential, their robustness and their ease of preparation. Relative to common metals such as Pt, IrOx formed electrochemically on bulk Ir (e.g., Ir wire) exhibits a high sensitivity towards the oxidation of H_2O_2 in CV experiments. Even lower potentials (0.35 V) can be used in chronoamperometric experiments, giving apparent Michaelis-Menten constants, K'_m, in the range of 11 – 16 mM and a maximum current of 0.5 – 2 mA cm^{-2}. The fact that a limiting oxidation current is reached at high H_2O_2 concentrations suggests that adsorption of H_2O_2 on IrOx occurs, analogous to Hall's study [12] at Pt. IrOx electrodes also offer a higher linear detection range for H_2O_2 oxidation (up

to at least 12 mM in CV experiments) than at other metallic electrodes.

In the present work, it has been shown that the kinetics of H_2O_2 oxidation at nanoparticulate IrOx films, deposited on various substrates by the deposition and subsequent electrochemical oxidation of Ir sols, are independent of the nature of the underlying electrode substrate. This has been inferred from the constancy of the observed $E_{1/2}$ values, which correlate with the reaction rate, and is also fully consistent with the highly conducting nature of IrOx films in their oxidized state.

In contrast, our studies with nanoparticulate IrOx films deposited on Pt, Ir and GC substrates have shown that the reduction of H_2O_2 at IrOx films occurs on the underlying electrode substrate. This is verified by the similarity in the $E_{1/2}$ values to what is observed on these bare substrate materials and is consistent with the electronically non-conducting properties of IrOx films at these lower potentials.

An unusual effect has also been reported in this work, in that the detection of H_2O_2 (however, only in the micromolar H_2O_2 range) can be realized by the catalytic growth of IrOx films, presumed to occur in an analogous manner as in the Fenton reaction [64]. This allows H_2O_2 detection over the entire range of potential of IrOx redox activity, which is a distinct advantage when considering potential interferents. Importantly, glucose can also be detected at IrOx-glucose oxidase biosensing electrodes by either tracking the H_2O_2 oxidation/reduction currents in the range of 1 to 12 mM H_2O_2, or by the unusual H_2O_2 induced growth of IrOx films in the μM range of H_2O_2 concentration.

6. Acknowledgements

The authors are grateful to the Natural Sciences and Engineering Research Council of Canada for the full support of this work. We are also very thankful to Professor Z. Galus for stimulating discussions and helpful suggestions during the preparation of this manuscript.

7. References

[1] C. W. Jones, *Applications of Hydrogen Peroxide and Derivatives*, RSC Clean Technology Monographs, ed. James H. Clark, the Royal Society of Chemistry, Cambridge **1999.**
[2] J. Wang, *Electroanalysis* **2001**, *13*, 983.
[3] M. Tierney, H. Kim, J. Tamada, R. Potts, *Electroanalysis* **2000**, *12*, 666.
[4] X. Lie, J. L. Zweier, *Free Radical Biol. Med.* **2001**, *31*, 894.
[5] A. Hickling, W. Wilson, *J. Electrochem. Soc.* **1951**, *98*, 4255.
[6] F. C. Anson, J. J. Lingane, *J. Am. Chem. Soc.* **1957**, *79*, 4901.
[7] J. J. Lingane, *J. Electroanal. Chem.* **1961**, *2*, 296.
[8] J. J. Lingane, P. J. Lingane, *J. Electroanal. Chem.* **1963**, *5*, 411.
[9] Y. L. Sandler, D. A. Pantier, *J. Electrochem. Soc.* **1965**, *112*, 9288.
[10] Y. Zhang, G. S. Wilson, *J. Electroanal. Chem.* **1993**, *345*, 253.
[11] E. Aschauer, R. Fasching, G. Urban, G. Nicolussi, W. Husinsky, *J. Electroanal. Chem.* **1995**, *381*, 143.
[12] S. B. Hall, E. A. Khudaish, A. L. Hart, *Electrochim. Acta* **1998**, *43*, 579.
[13] J. A. Cox, S. E. Gadd, B. K. Das, *J. Electroanal. Chem.* **1988**, *256*, 199.
[14] L. Gorton, *Anal. Chim. Acta* **1985**, *178*, 247.
[15] D. A. Johnston, M. F. Fardosi, D. H. Vaughan, *Electroanalysis* **1995**, *7*, 520.
[16] J. A. Cox, R. K. Jaworski, *Anal. Chem.* **1989**, *61*, 2176.
[17] R. K. Jaworski, J. A. Cox, B. R. Strohmeier, *J. Electroanal. Chem.* **1992**, *325*, 11.
[18] T. Ruzgas, E. Csöregi, J. Emnéus, L. Gorton, G. Marko-Varga, *Anal. Chim. Acta* **1996**, *330*, 123.
[19] A. A. Karaykin, *Electroanalysis* **2001**, *13*, 813.
[20] P. Mailley, *Talanta* **2001**, *55*, 1005.
[21] J. Wang, R. Li, M-S. Lin, *Electroanalysis* **1989**, *1*, 151.
[22] Y. Ikariyama, S. Yamauchi, T. Yukiashi, H. Ushioda, *J. Electrochem. Soc.* **1989**, *136*, 702.
[23] J. Wang, L. Angnes, *Anal. Chem.* **1992**, *64*, 456.
[24] J. Wang, J. Liu, L. Chen, F. Lu, *Anal. Chem.* **1994**, *66*, 3600.
[25] H. Sakslund, J. Wang, F. Lu, O. Hammerich, *J. Electroanal. Chem.* **1995**, *397*, 149.
[26] H. Sakslund, J. Wang, O. Hammerich, *J. Electroanal. Chem.* **1996**, *402*, 149.
[27] J. Wang, G. Rivas, M. Chicharro, *J. Electroanal. Chem.* **1997**, *439*, 55.
[28] M. C. Rodriguez, G. A. Rivas, *Electroanalysis* **1999**, *11*, 558.
[29] J. Liu, F. Lu, J. Wang, *Electrochem. Comm.* **1999**, *1*, 341.
[30] New F. Tian, G. Zhu, *Sens. Actuators B* **2002**, *86*, 266.
[31] E. Turkusic, K. Kalcher, K. Schachl, A. Komersova, M. Bartos, H. Moderegger, I. Svancara, K. Vytras, *Anal. Lett.* **2001**, *34*, 2633.
[32] T. Tatsuma, K. Tani, N. Oyama, H. H. Yeoh, *J. Electroanal. Chem.* **1996**, *407*, 155.
[33] R. D. Rauh, U. M. Twardoch, G. S. Jones, R. B. Jones, *Electrochem. Soc. Proc.* **1999**, *98–26*, 176.
[34] E. Abu Irhayem, H. Elzanowska, A. Jhas, B. Skrzynecka, V. I. Birss, *J. Electroanal. Chem.* **2002**, in press.
[35] P. J. Kulesza, L. R. Faulkner, *J. Electrochem. Soc.* **1989**, *136*, 707.
[36] P. J. Kulesza, B. Grzybowska, M. A. Malik, M. T. Galkowski, *J. Electrochem. Soc.* **1997**, *144*, 1911.
[37] J. A. Cox, K. Lewinski, *Talanta* **1992**, *40*, 1911.
[38] S. Gottesfeld, S. Srinivasan, *J. Electroanal. Chem.* **1978**, *86*, 89.
[39] S. H. Glarum, J. H. Marshal, *J. Electrochem. Soc.* **1980**, *127*,1467.
[40] J. Mozota, B. E. Conway, *J. Electrochem. Soc.* **1981**, *128*, 2142.
[41] L. D.Burke, D. P. Whelan, *J. Electroanal. Chem.* **1981**, *124*, 333.
[42] P. G. Pickup, V. I. Birss, *J. Electrochem. Soc.* **1988**, *135*, 126.
[43] P. G. Pickup, V. I. Birss, *J. Electroanal. Chem.* **1988**, *240*, 185.
[44] V. I. Birss, H. Elzanowska, S. Gottesfeld, *J. Electroanal. Chem.* **1991**, *318*, 327.
[45] H. Elzanowska, V. I. Birss, *J. Appl. Electrochem* **1993**, *23*, 646.
[46] H. Elzanowska, J. Segal, V. I. Birss, *Electrochim. Acta* **1999**, *44*, 4515.
[47] T. M. Silva, A. M. P. Simoes, M. G. S. Ferreira, M. Walls, M. D. Belo, *J. Electroanal. Chem.* **1998**, *441*, 5.
[48] L. S. Roblee, J. L. Lefko, S. B. Brummer, *J. Electrochem. Soc.* **1983**, *130*, 731.
[49] L. S. Robblee., T. L. Rose, in *Neural Prostheses, Fundamental Studies* (Eds: W. F. Agnew, D. B. McCreery), Prentice Hall, Englewood Cliffs, NJ **1990**, pp. 25–59.
[50] W. F. Agnew, T. G. H. Yuen, D. B. McCreery, L. A. Bullara, *Experimental Neurology* **1986**, *92*, 162.

[51] J. E. Baur, T. W. Spaine, *J. Electroanal. Chem.* **1998**, *443*, 208.
[52] V. I. Birss, H. Andreas, I. Serebrennikova, H. Elzanowska, *Electrochem. Solid-State Lett.* **1999**, *2*, 326.
[53] H. Andreas, H. Elzanowska, I. Serebrennikova, V. Birss *J. Electrochem. Soc.* **2000**, *147*, 4598.
[54] B. Le Drogoff, M. A. El Khakani, P. R. M. Silva, M. Chaker, A. K. Vijh, *Electroanalysis* **2001**, *13*, 1491.
[55] M. L. Hitchman, S. Ramanathan, *Analyst* **1988**, *113*, 35.
[56] M. L. Hitchman, S. Ramanathan, *Analyst* **1991**, *116*, 1131.
[57] M. L. Hitchman, S. Ramanathan, *Anal. Chim. Acta* **1992**, *263*, 53.
[58] R. M. Ianniello, A. M. Yacynych, *Anal. Chim. Acta* **1983**, *146*, 249.
[59] T. Krawczyk vel Krawczyk, M. Moszczynska, M. Trojanowicz, *Biosens. Bioelectron.* **2000**, *15*, 681.
[60] W. Matuszewski, M. Trojanowicz, *Electroanalysis* **1990**, *2*, 147.
[61] Y. Xian, W. Sun, J. Xue, M. Luo, L. Jin, *Anal. Chim. Acta* **1999**, *381*, 191.
[62] S. Reiter, K. Habermûller, W. Schuhmann, *Sens. Actuators B* **2001**, *79*, 150.
[63] E. Kosela, H. Elzanowska, W. Kutner, *Anal. Bioanal. Chem.* **2002**, *373*, 724
[64] D. T. Sawyer, *Coord. Chem. Rev.* **1997**, *165*, 297
[65] G. S. Nahor, P. Hapiot, P. Neta, A. Harriman, *J. Phys. Chem.* **1991**, *95*, 616.
[66] S. Reiter, K. Habermûller, W. Schumann, *Sensors & Actuators* **2001**, B79, 150
[67] V. I. Birss, R. Myers, H. Angerstein-Kozlowska, B. E. Conway, *J. Electrochem. Soc.* **1984**, *131*, 1502
[68] S. J. Xia, V. I. Birss, *J. Electroanal. Chem.* **2001**, *500*, 562.
[69] S. J. Xia, V. I. Birss, *Electrochim. Acta* **1998**, *44*, 467.
[70] S. J. Xia, V. I. Birss, *Electrochim. Acta* **2000**, *45*, 3659.